External mechanical cues reveal core molecular pathway behind tissue bending in plants

Authors: Anirban Baral[1,*], Emily Morris[2,b], Bibek Aryal[1,3], Kristoffer Jonsson[1], Stéphane Verger[1], Tongda Xu[4], Malcolm Bennett[2], Olivier Hamant[5], Rishikesh P. Bhalerao[1,*,†]

Affiliations:

[1]Umeå Plant Science Centre, Department of Forest Genetics and Plant Physiology, Swedish University of Agricultural Sciences, 901 87 Umeå, Sweden,

[2]Centre for Plant Integrative Biology, University of Nottingham, Nottingham LE12 SRD, UK,

[3]Beijing Advanced Innovation Centre for Tree Breeding by Molecular Design, Beijing Forestry University, Beijing 100083, China,

[4]FAFU-Joint Centre, Horticulture and Metabolic Biology Centre, Haixia Institute of Science and Technology, Fujian Agriculture and Forestry University, Fuzhou, Fujian 350002, China,

[5]Laboratoire de Reproduction et Développement des Plantes, Université de Lyon, ENS de Lyon, UCBL, INRA, CNRS, 46 Allée d'Italie, 69364, Lyon, Cedex 07, France,

[b]Current address: Oxford University Innovation, Buxton Court, 3 West Way, Oxford OX20JB, UK.

[†]Lead contact: Rishikesh P Bhalerao.

*For correspondence: abaral1986@gmail.com (A.B); Rishi.Bhalerao@slu.se (R.P.B)

Summary

Tissue folding is a central building block of plant and animal morphogenesis. In dicotyledonous plants, hypocotyl folds to form hook after seedling germination that protects their aerial stem cell niche during emergence from soil. Auxin response factors and auxin transport are classically thought to play a key role in this process. Here we show that the microtubule-severing enzyme katanin contributes to hook formation. However, by exposing hypocotyls to external mechanical cues mimicking the natural soil environment, we reveal that auxin response factors ARF7/ARF19, auxin influx carriers, and katanin are dispensable for apical hook formation, indicating that these factors primarily play the role of catalyzers of tissue bending in the absence of external mechanical cues. Instead, our results reveal the key roles of the non-canonical TMK-mediated auxin pathway, PIN efflux carriers and cellulose microfibrils as components of the core pathway behind hook formation in presence or absence of external mechanical cues.

Keywords

Tissue folding, Differential growth, mechanical cues, microtubule, cellulose, auxin.

Introduction

Tissue folding is an essential feature of body plan development across kingdoms. In animals, tissue rearrangements can generate patterns of tension and compression, which in turn contribute to tissue invagination during gastrulation, through the actomyosin mediated response to forces (Sherrard, et al., 2010; Martin, et al., 2009; Farge, 2003). Interestingly, such intrinsic mechanical cues can be artificially mimicked by external mechanical cues in the form of local indentations; even rescuing tissue invagination defects in *Drosophila* myosin mutants (Pouille, et al., 2009). This calls for an investigation of the relative contribution of intrinsic and external mechanical cues to development. In animals the core developmental plan is laid out in the embryonic stage, and since animal embryos are usually embedded in a protective shell, such external cues are likely to be filtered out. In contrast, the postembryonic development of plants is constantly exposed to both internal and external mechanical constraints Here we investigate how plants cope with such conflicting cues to control tissue folding.

The presence of stiff cell walls and high turgor pressure in plants limit certain mechanisms of differential growth such as cell migration and cell contraction. However, because plant cells are tightly attached to one another through their contiguous walls, local differences in cell elongation is employed to create pronounced deformations in tissue and organ shape (Echevin, et al., 2019). In keeping with their sessile lifestyle, land plants have also acquired the unique ability to substantially alter their shape and form to adapt to their environment. The genetic and biochemical pathways that regulate differential growth in plants**,** and their modulation by exogenous cues**,** have been investigated in numerous studies; reviewed in (Chaiwanon, et al., 2016). In addition to biochemical signals, a critical role for mechanical signals in regulating plant development is emerging. Touch or wind has a genome-wide impact on the transcriptome, leading to wall stiffening and reduced stature (Braam, 2005) Mechanical signals can also arise internally: turgor pressure puts walls and tissues under tension (Kutschera and Nikas, 2007), and mechanical conflicts arise between cells and tissues with different growth parameters, as seen in shoot apical meristems (Uyttewaal, et al., 2012), sepals (Hervieux, et al., 2017) and leaves (Huang, et al., 2018).

Hypocotyl bending to form an (apical) hook is facilitated by differential cell elongation. Polar transport-mediated accumulation of auxin on one side of the hypocotyl restricts the elongation of epidermal cells (Abbas, et al., 2013), forming the concave side of the apical hook. Such tissue folding reflects a mechanical conflict across the structure (Landrein, et al., 2015). Interestingly, the apical hook forms during germination in the absence of external constraints in petri dishes, while under native growth conditions, hook development proceeds under mechanical constraints imposed by the soil (Abbas, et al., 2013). We are using tissue bending in the hypocotyl during seed germination as an experimental model to study how exposure to exogenous cues from mechanical constraints during soil emergence as well as endogenous cues can modulate shape change through differential growth and tissue folding.

In plants, cortical microtubules (CMTs) are key players in morphogenesis; they mediate the deposition of cellulose microfibrils and confer directionality during cell elongation. Interestingly, CMTs have been shown to align with directions of maximal tensile stress that tissue shape and/ or growth imposes (Hamant, et al., 2019; Sampathkumar, et al., 2014; Uyttewaal, et al., 2012). However, exogenously applied force can override the endogenous stress pattern and reorient CMTs (Robinson and Kuhlemeier, 2018; Uyttewaal, et al., 2012). The protein katanin plays a key role in promoting CMT self-organization in response to such cues, by severing nascent microtubule branches and microtubule crossovers as well as promoting microtubule bundling (Luptovciak, et al., 2017). In loss-of-function katanin mutants, CMT arrays are slow to self-organize in parallel bundles and thus usually appear disorganized (Bouquin, et al., 2003). CMTs in these mutants react slowly to both endogenous and exogenous mechanical cues (Hervieux, et al., 2017; Sampathkumar, et al., 2014; Uyttewaal, et al., 2012). However, attaining anisotropic CMT orientation even in the absence of katanin activity is theoretically possible through growth, cell shape and geometry-induced self-organization of CMTs (Chakrabortty, et al., 2018) and from directional stabilization of CMT arrays by prolonged exogenous mechanical cues (Hamant, et al., 2019). It seems therefore that exogenous and endogenous mechanical stress can act in synergy to control CMT organization. However, the significance of this balance of growth processes remains to be demonstrated.

Through the study of hypocotyl bending during hook formation under mechanical constraints imposed by soil**,** we identified a role for dynamic rearrangement of CMTs in tissue folding, in response to both internal and external mechanical cues. Importantly**,** our results demonstrate that external mechanical constraints can rescue tissue folding defects in the katanin mutants. The associated mechanism is dependent on cellulose microfibril organization and on the polar auxin transport machinery, and it requires an alternative auxin response pathway mediated via the TMK receptor kinase to facilitate tissue bending and apical hook formation.

Results:

Apical hook formation depends on katanin-dependent microtubule organization

To assess the mechanisms underlying tissue bending under mechanical constraints we used apical hook development as a model. Since CMTs are key morphogenetic regulators, we first assessed their role in hypocotyl bending and hook development. We compared hook formation in WT and the *ktn1-5* mutant (Lin, et al., 2013) which lacks the microtubule-severing enzyme katanin. Whereas WT seedlings formed closed apical hooks approximately 30 Hrs after germination (Figure 1A, left), *ktn1-5* mutant seedlings could not achieve hypocotyl bending and their hooks were open (Figure 1A, right). Using time-lapse infrared imaging (Boutte, et al., 2013) we observed that *in vitro*-grown WT seedlings formed closed apical hooks by progressive bending the hypocotyl within 24-26 Hrs of germination**.** After 28 Hrs, hooks of all the WT seedlings were closed (hook angle of 180°) (Figure. 1B). In contrast, *ktn1-5* seedlings growing on the agar surface were unable to form this bend and 28 Hrs after germination their hook angles were much smaller (53.89 ± 25.63°, n = 20), (Figure. 1B)

CMT organization has been associated with stem curvature in response to gravistimulation or forced bending (Ikushima and Shimmen, 2005). Here we characterized CMT arrangement in WT hooks compared to *ktn1-5.* We used the reporter microtubule-associated protein 4 fused with green fluorescent protein (GFP-MAP4) to visualize microtubules (Marc, et al., 1998) and the FibrilTool plugin (Boudaoud, et al., 2014) to quantify CMT arrangement (array anisotropy) across the hypocotyl. In WT hooks

133 CMT arrays were significantly more anisotropic (anisotropy value 0.27 ± 0.009 SEM, n =
134 250 cells) on the convex side of the hook than on the concave side (anisotropy value 0.18
135 ± 0.001 SEM, n = 251 cells) (Figure. 1C, 1D). In contrast, CMT arrays in *ktn1-5* showed
136 significant reduction in anisotropy and there was little difference in array anisotropy across
137 the two sides of the hypocotyl (Figure. 1E, 1F, side1 *vs* side2; anisotropy values 0.084 ±
138 0.003 SEM, n = 221 cells and 0.085 ± 0.002 SEM, n = 179 cells). These results suggest
139 that the difference in CMT organization on the two sides of the hypocotyl is associated
140 with tissue bending during hook development and its disruption is associated with defects
141 in hook formation.

142 **Apical hook defect in *katanin mutant* can be rescued by external constraints**

143 Typically, upon germination, emerging seedlings are exposed to physical, biochemical
144 and biological constraints by the soil. Hence we investigated the role of microtubules in
145 hook formation in wild type and *ktn1-5* under natural conditions by germinating seeds
146 within sterile soil and imaging hook formation using non-invasive X-ray microcomputed
147 tomography (Orman-Ligeza, et al., 2018). Intriguingly, hypocotyl bending and formation
148 of closed hooks were observed in *ktn1-5* seedlings growing through the soil (Figure. 1G).
149 Thus, despite the inability to form a hook on the agar surface, during growth in soil (a
150 more natural condition for germinating seeds), the *ktn1-5* hypocotyl was able to bend and
151 form a hook.

152 To focus on the physical contribution of the soil to this response, we investigated hook
153 formation by germinating seeds inside agar (as a proxy for soil). Using time-lapse infrared
154 imaging (Boutte, et al., 2013), we observed that hooks of all the WT seedlings were closed
155 (hook angle of 180^0) both on the surface and in agar. Hook angles of constrained (agar-
156 grown) and free (surface-grown) WT seedlings were similar, suggesting that mechanical
157 constraints do not amplify hook bending (Figure. 1B). Intriguingly, germination in agar
158 significantly alleviated hook defects in *ktn1-5* seedlings and after 28 Hrs post-germination
159 their hook angles were much larger (162.06 ± 17.8°, n= 20), when compared to surface-
160 grown *ktn1-5* seedlings, i.e. those not exposed to external mechanical constraints (Figure.
161 1B).

162

163 ***katanin* rescue by external constraints relies on microtubule dynamics**

164 The developmental defects seen in the *ktn1-5* mutant are attributed to the CMT
165 disorganization associated with loss of the microtubule-severing and bundling activities
166 of katanin (Luptovciak, et al., 2017). In the most parsimonious scenario, reestablishment
167 of apical hook formation by mechanical cues in *ktn1-5* could suggest that microtubules
168 are not essential for bending in response to mechanical cues during growth in soil. To
169 check this hypothesis, we used pharmacological and genetic approaches. Treatment with
170 low concentrations of the microtubule-depolymerizing drug oryzalin (200 nM) or the
171 microtubule-stabilizing drug paclitaxel (50 nM), which did not affect WT seedlings (Figure.
172 S1A, S1C), completely abolished hook formation in *ktn1-5* seedlings grown in agar
173 (Figure. S1B, S1D). Additionally, genetically perturbing CMT rearrangement by
174 introducing the *tua5*^{D251N} mutation (which slows down microtubule dynamics) (Ishida, et
175 al., 2007) in *ktn1-5* also abolished hook formation in response to mechanical constraints
176 (Figure. S1F). Thus, even in the absence of katanin, microtubule dynamics is required for
177 apical hook formation.
178 When mechanical stress levels are increased in the shoot apical meristem (e.g. upon wall
179 weakening with the cellulose synthase inhibitor isoxaben), CMTs can exhibit WT-like
180 behavior in a *katanin* mutant, where they can reorient around a single cell ablation as in
181 WT (Uyttewaal, et al., 2012). We reasoned that soil, or agar gel, may provide a
182 mechanical cue strong enough to compensate for the slower CMT dynamics in the
183 *katanin* mutant. To test this hypothesis, we investigated whether constrained growth in
184 agar could facilitate a difference in CMT organization in the *ktn1-5* mutant. In contrast to
185 the lack of significant difference in CMT array anisotropy in surface-grown *ktn1-5*
186 seedlings, growth under mechanical constraints resulted in a significant difference in CMT
187 array anisotropy between the two sides of *ktn1-5* mutant hypocotyls (Figure. 1H, 1I;
188 anisotropy value of 0.15 ± 0.003 SEM, n = 315 cells on convex side *vs* 0.09 ± 0.002 SEM,
189 n = 360 cells on concave side). Note that absolute anisotropy values were lower in *ktn1-*
190 *5* than in the WT, suggesting that the relative difference in CMT behavior between the
191 two sides of the hypocotyl may be sufficient for tissue bending. Taken together our results
192 indicate that external mechanical cues can catalyze the formation of differential CMT
193 organization on both sides of the hypocotyl to induce tissue bending.

194

195 **Cellulose microfibril deposition is critical for mechanically-induced hook formation**

196 From the close association of CMTs and cellulose synthase complexes (Paredez, et al.,
197 2006) it can be surmised that CMTs would guide the deposition of cellulose microfibrils
198 to promote hook formation. To formally check this, we first examined hook formation in
199 two mutants with altered cellulose content and cellulose organization: the cellulose
200 synthase A1 (CesA1) mutant *any1***,** with reduced crystalline cellulose content (Fujita, et
201 al., 2013)**,** and the cellulose synthase interacting 1 (CSI1) protein deficient mutant *pom2-*
202 *8* (Bringmann, et al., 2012)**,** featuring altered cellulose fiber orientation arising from the
203 partial decoupling of CesA complex from CMTs. As expected, both *any1* and *pom2-8*
204 mutants had defects in hook formation (Figure 2A, 2B). However, unlike *ktn1-5,* hook
205 formation in *any1* and *pom2-8* mutants was not appreciably suppressed by growth inside
206 agar (Figure. 2A, 2B). These results further suggest that the rescue of the *ktn1-5* hook
207 defect by growth in agar requires CMT-guided cellulose deposition. To test this, we
208 introduced *any1* and *pom2-8* mutations into the *ktn1-5* background. Hook formation could
209 not be restored in agar-grown *ktn1-5 any1* or *ktn1-5 pom2-8* double mutant seedlings
210 (Figure. 2C, 2D). We also found that hook formation in agar-grown *ktn1-5* seedlings was
211 hypersensitive (Figure. S2) to 100 nM 2,6-dichlorobenzonitrile (DCB), a cellulose
212 biosynthesis inhibitor (DeBolt, et al., 2007). Hence, both genetic and pharmacological
213 approaches demonstrate the crucial role of cellulose organization in mediating the
214 bending required for hook formation in response to mechanical cues.

215 **Differential growth mediated by mechanical cues is dependent on auxin response**
216 **asymmetry**

217 Hypocotyl bending during apical hook formation results primarily from differences in
218 epidermal cell elongation between the sides (Raz and Koornneef, 2001). Consistent with
219 this, and because there is limited cell division at this stage (Zadnikova, et al., 2016),
220 epidermal cell length was significantly different between the concave (34.26 ± 0.11 μm
221 SEM, n = 250 cells) and convex (61.39 ± 2.86 μm SEM, n = 251 cells) sides of the WT
222 hook (Figure 3A). In sharp contrast, epidermal cell lengths in *ktn1-5* were similar on both

223 sides of the hypocotyl (Figure. 3B, side 1 vs side 2); cell length 53.85 ± 1.592 μm SEM,
224 n = 221 cells and 61.90 ± 2.02 μm SEM, n = 179 cells. As expected, when grown inside
225 agar, cell length difference across the hypocotyl was re-established in *ktn1-5* seedlings
226 (Figure. 3C); cell length of 33.02 ± 0.64 μm SEM, n = 360 cells on the concave side *vs*
227 63.24 ± 1.2 μm SEM, n = 351cells on the convex side. The cells on the concave (inner)
228 side of mechanically constrained *ktn1-5* seedlings were significantly smaller than cells on
229 either side of surface-grown *ktn1-5* seedlings (Figure. 3D). These results suggest that
230 growth asymmetry mediated by repression of growth on one side can be reestablished in
231 *ktn1-5* seedlings grown under mechanical constraint.
232 The repression and slower rate of cell elongation can be attributed to auxin response
233 maxima forming on the concave side (Zadnikova, et al., 2010). Mechanical constraints in
234 agar-grown hypocotyls could simply deform the hypocotyl resulting in bending through a
235 direct impact on CMTs. Alternatively, mechanical cues may influence the auxin response,
236 modifying differential growth, and indirectly affecting CMTs. To address this, we first
237 investigated whether impaired hook formation in *ktn1-5* seedlings is due to attenuation of
238 the auxin response. In WT hooks, auxin response maxima, visualized using the synthetic
239 auxin reporter DR5:: Venus-N7 (Heisler, et al., 2005), were seen only on the concave
240 side (Figure. 3E, left): whereas the *ktn1-5* seedlings failed to establish this asymmetry;
241 DR5:: Venus-N7 signals were seen on both sides of the hypocotyl (Figure. 3E, middle).
242 We then investigated whether constrained growth in agar gel could reestablish DR5::
243 Venus-N7 signal asymmetry in a katanin-independent manner. In *ktn1-5* seedlings grown
244 inside agar, the DR5:: Venus-N7 signal was observed only on the concave side (Figure.
245 3E, right). Lastly, microtubule perturbation with 200 nM oryzalin abolished establishment
246 of DR5:: Venus-N7 signal asymmetry in *ktn1-5* seedlings grown inside agar (Figure. S3B).
247 These data suggest that mechanical constraints in agar-grown hypocotyls induce hook
248 formation by establishing auxin response asymmetry, and the resulting mechanical
249 conflict would be strong enough to override reduced CMT dynamics in the *katanin* mutant.
250
251

252 **Mechanical constraints can modulate polar auxin transport during apical hook**
253 **formation**

254 To decipher the link between external mechanical constraints and differential auxin
255 response in the apical hook, we next analyzed the contribution of auxin transporters.
256 Auxin influx carriers of the AUX/ LAX family are thought to play an important role in auxin
257 response asymmetry in the apical hook (Vandenbussche, et al., 2010). Consistently, hook
258 formation was severely affected in the *aux1 lax1 lax2 lax3* quadruple mutant when grown
259 on the surface, mimicking the *ktn1*-5 mutant phenotype (Figure. S4A). As observed for
260 *ktn1-5*, growth inside agar could restore hook formation in this *aux/ lax* quadruple mutant
261 (Figure. S4A), as observed for *ktn1-5*. Thus hook formation does not require AUX/LAX
262 auxin influx carriers.
263 The efflux carriers of the PIN-FORMED (PIN) family are also thought to be required for
264 hook formation (Zadnikova, et al., 2010). Similar to AUX/ LAX carriers, hook formation
265 was also completely abolished in the *pin1347* quadruple mutant when grown on the
266 surface (Figure. S4B). However, in contrast with *aux/ lax* or *ktn1-5* mutants, hook
267 formation did not occur in *pin1347* (Figure. S4B) even when grown inside agar. Thus
268 external mechanical cues can override both katanin-dependent CMT dynamics and AUX/
269 LAX-dependent auxin influx, but they require PIN auxin transporters for hook formation.
270 Tissue- and cell-type-specific polar localization of PIN transporters is critical for the
271 directional flow of auxin (Grunewald and Friml, 2010). For the PINs implicated in hook
272 development (PIN1, 3, 4 and 7), PIN4-GFP signal could be detected only in the epidermal
273 cells. The localization of PIN4-GFP was strongly polar with preferential localization to
274 transverse membranes compared to the lateral sides (Figure 4A, left; Figure. S5A, S5B).
275 PIN3-GFP signal could be detected in epidermal and cortical cells, with significantly
276 stronger signal on transverse membranes compared to lateral sides in the epidermis
277 (Figure 4B, left; Figure. S5A, S5C) and exclusively transverse localization in cortical cells
278 (Figure 4C, left). In surface-grown *ktn1-5* mutant seedlings, the polarities of PIN3-GFP
279 and PIN4-GFP were strongly perturbed. Localization of both PIN3 and PIN4 GFP was
280 significantly enhanced at the lateral membranes of epidermal cells in *ktn1-5* compared to
281 WT (Figure. 4A, 4B, middle; Figure. S5B, S5C). Moreover, PIN3-GFP was mislocalized
282 to lateral membranes in cortical cells of *ktn1-5* (Figure 4C, middle). Intriguingly, PIN1-

GFP displayed a unique spatially-restricted localization pattern in the WT hook (Zadnikova, et al., 2010). PIN1-GFP signal could be detected on the plasma membrane only in cells on the concave side (Figure 4E, left). In the *ktn1-5* hook region, however, PIN1-GFP was completely absent from plasma membrane but it could be detected in punctate intracellular structures (Figure 4E, middle). PIN7-GFP signal could be detected only in epidermal cells, which showed nonpolar localization (Figure S5). In contrast to PIN 1, 3 and 4, neither the localization nor the intensity of PIN7 underwent any change in *ktn1-5* (Figure S6D, S6E). We then examined whether mechanical cues can mediate the localization of PIN transporters required to induce hook formation. When grown inside agar, the polarity of PIN4-GFP in epidermis (Figure 4A right; Figure. S6B) and PIN3-GFP in both epidermis (Figure 4B, right; Figure. S6C) and cortex (Figure. 4C, right) was partially but significantly restored in *ktn1-5*. Furthermore, PIN1-GFP signal was now primarily on the plasma membrane of cells on the concave side in *ktn1-5*, resembling the localization pattern seen in WT hooks (Figure. 4D, right).

Thus, the genetic analysis of *pin* mutants and localization analysis of PINs strongly supports our scenario: mechanical constraints associated with growth in agar would mediate the recruitment (PIN1) and polarity (PIN3, PIN4) of auxin efflux carrier, thereby generating a differential auxin response and differential cell elongation; the resulting mechanical conflicts would be strong enough for CMTs to align with the directions of mechanical stress, and maintain tissue bending, even compensating the absence of the catalyzer of CMT self-organization, katanin.

Cellulose microfibril deposition is critical for differential auxin response in the hook

As mentioned above, cellulose acts downstream of CMTs to control directional cell growth, through the CMT-CesA nexus (Paredez, et al., 2006). Interestingly, a role for CesA activity in the regulation of PIN1 localization has also been reported (Feraru, et al., 2011). This would put cellulose upstream of the CMT response to mechanical cues, via the formation of differential auxin patterns and resulting mechanical conflicts. This prompted us to investigate whether external cues require cellulose microfibrils for the establishment of PIN polarities and auxin response. First, we investigated whether the

314 cellulose mutants fail to establish the auxin response maxima critical for hook formation.
315 In contrast to WT plants**,** with DR5:: Venus-N7 signal only on the concave side, Figure.
316 5A), the DR5:: Venus-N7 pattern in seedlings of both the cellulose mutants, *any1* and
317 *pom2-8***,** was altered and diffuse (Figure. 5B, 5C) suggesting a defect in establishing an
318 auxin response maximum when cellulose deposition is affected. Analysis of the
319 localization of PIN efflux carriers showed epidermal polarity of PIN3-GFP and PIN4-GFP
320 was significantly reduced in *any1* and *pom2-8* compared to WT (Figure. 5D, 5E, S6A,
321 S6B). PIN3-GFP was also found on lateral membranes of cortical cells in *any1* and *pom2-*
322 *8* hooks (Figure. 5F), similar to *ktn1-5* seedlings. Looking at PIN1-GFP, we found that**,**
323 similar to *ktn1-5*, GFP signal was absent from plasma membrane but present in
324 intracellular punctate structures (Figure. 5G). These results are consistent with a scenario
325 in which cellulose is required for the polarity of PIN auxin efflux carrier and the resulting
326 auxin response patterns; in that scenario, cellulose would indirectly control the CMT
327 response to external mechanical cues, via its impact on auxin distribution.
328

329 **Signaling mediated by TMK1 and 4 is necessary for mechanosensitive hook**
330 **formation**

331 Two major pathways have been reported to mediate the auxin response in the hook. The
332 transcription factors ARF7/ ARF19 mediate the canonical auxin response pathway, and
333 as a result the *arf7 arf19* double mutant displays a strong hook defect (Zadnikova, et al.,
334 2010). However, we found that the marked hook defects of the *arf7 arf19* double mutant
335 could be rescued by constraining growth in agar gel (Figure. S7A). Furthermore, the *ktn1-*
336 *5 arf7 arf19* triple mutant displayed a similar response to mechanical cues as the *ktn1-5*
337 single mutant with respect to hook formation (Figure. S7B). This suggests that hook
338 formation in response to mechanical cues does not require ARF7 and ARF19 activity.
339 A recent study suggests that the plasma membrane localized receptor TMK1 is a
340 component of a non-canonical auxin signaling pathway operating in the apical hook (Cao,
341 et al., 2019). Perception of higher levels of auxin causes cleavage and nuclear
342 translocation of a C-terminal fragment of TMK1 specifically on the concave side of the
343 hook, subsequently repressing growth of these cells through stabilization of specific
344 nuclear AUX/ IAA transcription factors. Since neither ARF7 and ARF19 was required for

345 hook formation in response to external mechanical cues, we investigated whether this
346 pathway acts via TMKs.
347 The *tmk1* null mutant displays a defect in hook maintenance but not in hook formation.
348 Nor do the loss of three remaining members of the TMK family cause any appreciable
349 hook phenotypes (Cao, et al., 2019). However, the functional redundancy between TMK1
350 and TMK4 (Dai, et al., 2013) prompted us to look into hook formation in the *tmk1tmk4*
351 double mutant. This mutant showed a clear hook formation defect, as well as defects in
352 auxin response asymmetry as visualized with DR5:: Venus-N7. Strikingly, this response
353 could not be rescued by constraining growth in agar gel (Figure. 6A-C). These results
354 strongly suggest that hook formation in response to growth under mechanical constraints
355 depends on the TMK pathway. Taken together, our observations suggest that the
356 components of the non-canonical auxin response pathway, TMK1 and TMK4, act
357 redundantly and are required to mediate bending in response to mechanical cues during
358 hook formation.
359

360 **Discussion**

361 A unique feature of morphogenesis in plants is the postembryonic adaptability to their
362 environment. Formation of the hook during early seedling establishment is an example of
363 such an adaptive response, protecting the fragile shoot apical meristem during soil
364 emergence. In this study we show that asymmetry in cell elongation, the auxin response
365 and CMT behavior drive differential growth during hook formation. Although these
366 responses are absent in the *katanin* mutant, we demonstrate that katanin only catalyzes
367 this response: external mechanical cues can generate a hook independent of katanin.
368 Recently, an important role of mechanical cues originating from gravitropic bending of the
369 root to the generation of auxin asymmetry has been proposed during hook formation (Zhu,
370 et al., 2019). Our results provide support for this suggestion and reveal a scenario
371 involving auxin efflux carriers, and not auxin influx carriers, and in which CMTs react to
372 external mechanical cues and a TMK-dependent auxin response pathway to promote
373 hook formation.
374 Although apical hook formation has been studied extensively as a model for differential
375 cell elongation and underlying hormonal pathways and transcriptional networks

376 (Mazzella, et al., 2014), most of these studies were performed by growing seeds on the
377 surface of agar. Under these laboratory conditions, the hypocotyl is not subject to external
378 cues akin to mechanical constraints imposed by soil. As a result, the role of exogenous
379 mechanical cues in hypocotyl bending to form a hook has not been explored in detail. By
380 introducing external mechanical cues in the form of agar-grown hypocotyls, we reveal
381 that three key factors, auxin response factors, auxin influx carriers and microtubule-
382 severing enzyme katanin are dispensable for apical hook formation. By challenging the
383 intrinsic genetic control of apical hook formation with external mechanical cues, we could
384 extract the key players of tissue bending in the context of apical hook formation.
385 How plant cells may differentiate between external (e.g. wind, touch) and internal
386 mechanical cues is subject to debate. Plant cells may in fact use the same pathways to
387 respond to mechanical forces, independent of the cause of mechanical stress (Hamant
388 and Haswell, 2017). In particular, artificial mechanical perturbations are classically
389 performed to check whether plant cells can orient their CMTs with the direction of maximal
390 tensile stress, mimicking the CMT response to growth- and shape-derived stress in
391 control tissues (Robinson and Kuhlemeier, 2018; Sampathkumar, et al., 2014; Hamant,
392 et al., 2008). Yet, the associated mechanotransduction pathways have remained
393 unknown so far. Among the candidate mechanisms to exclude, CMTs seem to align with
394 local mechanical stress reorientation in the shoot apical meristem even when calcium
395 signals are blocked (Li, et al., 2019) or when auxin gradients are largely impaired (Heisler,
396 et al., 2010) Therefore it has been proposed that CMTs may be their own
397 mechanosensors (Hamant, et al., 2019) echoing what has been proposed for actin in
398 animals (Yu, et al., 2017; Risca, et al., 2012) and building on evidence from stretched
399 microtubules *in vitro* (Franck, et al., 2007). Yet, the integration of such behaviors in
400 development requires a coordinator, a role that could be played by auxin and mediated
401 by a TMK dependent, non-canonical auxin response pathway.
402 Several mechanisms mediate the formation of ordered CMT arrays, including
403 polymerization/ depolymerization, bundling and severing (Dixit and Cyr, 2004).
404 Microtubule severing by katanin has been shown to promote CMT anisotropy in several
405 studies; reviewed in (Luptovciak, et al., 2017) and indeed our data also show that in the
406 absence of katanin, CMT arrays are more isotropic. However, we found that mechanical

407 cues can promote CMT anisotropy in the absence of katanin. At first glance, our
408 observations are in conflict with the role of katanin in mediating the response of CMTs to
409 external mechanical cues (Sampathkumar, et al., 2014). However, our data are consistent
410 with slower but pronounced reorganization of CMTs in meristems of katanin mutants
411 subjected to prolonged mechanical cues (Louveaux, et al., 2016; Uyttewaal, et al., 2012).
412 Katanin-independent CMT reorganization can happen by motor protein mediated
413 reorientation of CMTs (Inoue, et al., 2016). Also, altered polymerization/ depolymerization
414 of MTs by mechanical stress can rearrange CMTs in absence of katanin activity (Trushko,
415 et al., 2013). Indeed, hypersensitivity of mechanical constrain mediated hook formation
416 in *ktn1-5* seedlings towards MT-depolymerizing and polymerizing drugs (oryzalin and
417 paclitaxel) point towards an important role of microtubule polymerization/
418 depolymerization in katanin-independent CMT reorganization.
419 CMT disorganization associated with loss of katanin function alters the organization of
420 overlaying cellulose microfibrils (Burk and Ye, 2002); this, together with the alteration of
421 PIN1 polarity associated with cellulose defects (Feraru, et al., 2011), raises the possibility
422 that the PIN localization defects seen in the *ktn1-5* mutant stems from cellulose
423 disorganization. That PIN mislocalization is similar in *any1* and *pom2-8* mutants supports
424 the importance of cellulose organization in guiding the PIN polarity necessary for hook
425 formation. Furthermore, it has been reported that PIN1 localization at the plasma
426 membrane is sensitive to mechanical stress (Nakayama, et al., 2012). It is conceivable
427 that CMTs and cellulose regulate PIN localization and auxin asymmetry formation
428 indirectly, by mediating mechanical stress associated with tissue folding. Nonetheless,
429 our study reveals that CMTs and cellulose, by acting as mediators of mechanical stress,
430 can guide key developmental processes such as tissue folding in plants by modulating
431 PIN localization and auxin asymmetry. The localization of TMKs at the cell periphery, their
432 role in auxin perception (Dai, et al., 2013) together with their role in apical hook formation,
433 opens the possibility that these receptors may act as an integrator of both biochemical
434 (auxin) and mechanical cues.
435 To conclude, the analysis of apical hook formation in the presence of external mechanical
436 cues are reminiscent of observations in *Drosophila*. During gastrulation, tissue
437 deformation through external mechanical cues can compensate defective myosin in

Drosophila (Pouille, et al., 2009). Here we find that stiff agar can trigger apical hook formation, even when CMT dynamics is reduced in the katanin mutant. Beyond the parallel between plants and animals, such approaches further show how challenging development with external mechanical cues can be a productive way to dissect the molecular pathways behind morphogenesis, and identify the core players

Acknowledgements:

We thank Eva Benkova, Geoffrey O. Wasteneys, Ranjan Swarup and Enrico Scarpella for sharing published materials. Our sincere thanks to Anne-Lise Routier-Kierzkowska and Daniel Kierzkowski for reading through the manuscript and providing valuable inputs. A.B thanks the Wenner-Gren foundation for a travel fellowship. This work was funded by grants from the Knut and Allice Wallenberg Foundation awarded to R.P.B

Author Contributions

A.B, R.P.B, O.H and M.B conceived the project and designed experiments. E.M performed the MicroCT experiments. B.A contributed the *auxlax* quadruple mutant data. A.B performed all other experiments and analysed the data. K.J contributed to initial screening of the *katanin* mutant phenotypes and provided valuable discussions. T.X provided critical intellectual inputs. S.V provided the Surfcut analysis tool and provided critical inputs. A.B, R.P.B, O.H and M.B wrote the paper. R.P.B guided the research.

Declaration of Interests

The authors declare no competing interests.

Star methods:

Plant material

Arabidopsis thaliana ecotype Col-0 was used as wild type (WT) control in all experiments. The mutant lines *ktn1-5* (Lin, et al., 2013), *any1* (Fujita, et al., 2013), *pom2-8* (Bringmann, et al., 2012), *tua5*^{D251N} (Ishida, et al., 2007), *pin1 3 4 7* (Belteton, et al., 2018), *aux1 lax1 lax2 lax3* (Vandenbussche, et al., 2010) *arf7arf19* (Okushima, et al., 2005) *tmk1tmk4* (Dai, et al., 2013) and fluorescent reporter lines 35S:: GFP-MAP4 (Marc, et al., 1998), PIN1:: PIN1-GFP, PIN3:: PIN3-GFP (Zadnikova, et al., 2010), PIN4:: PIN4-GFP, PIN7:: PIN7-

466 GFP (Belteton, et al., 2018), DR5:: Venus-N7 (Heisler, et al., 2005) lines have been
467 described previously.

468 **Time lapse analysis of apical hook development**

469 For time lapse imaging of apical hook development, seegs sown on surface of agar plates
470 or embedded in agar (1/2 Murashige and Skoog medium, 1% plant agar, Duchefa
471 Biochemie), were grown on vertical plates in the dark at 21°C illuminated with far infra-
472 red-light (850 nm). Seedlings were photographed every hour using a Canon D50 camera
473 without the infrared filter. Hook angles were measured as previously described (Boutte,
474 et al., 2013) using Image J/Fiji.

475 **CMT imaging and quantification**

476 Dark-grown WT or ktn1-5 mutant plants expressing GFP-MAP4 were imaged with a Zeiss
477 LSM 880 confocal microscope using airyscan scanning. Post-acquisition, the images
478 were processed using the airyscan processing module incorporated in the Zen 2.3
479 software. The cortical signal (0-10 μm depth) was extracted from the stacks using the
480 Surfcut pipeline incorporated in the Image J/Fiji program (Erguvan, et al., 2019). CMT
481 anisotropy was measured using the FibrilTool plugin (Boudaoud, et al., 2014) in Image
482 J/Fiji.

483 **Confocal laser-scanning microscopy and quantification of fluorescence intensity**

484 Samples were imaged using a Ziess LSM 880 confocal laser scanning microscope. GFP,
485 and YFP, were excited by 488 and 514 lasers respectively and respective fluorescence
486 emissions were detected at 492-540 and 518-560 nm windows. Images for plasma
487 membrane fluorescence intensity quantification of PIN1-GFP, PIN3-GFP, PIN4-GFP and
488 PIN7-GFP in hook epidermal cells of were captured under identical acquisition
489 parameters (laser power, photomultiplier gain, offset, zoom, and resolution) between WT
490 and mutants. Polarity index was calculated as the ratio of basal/ lateral intensities.
491 Statistical analysis methods are described in figure legends.

492 **X-Ray microcomputed tomography**

493 WT and *ktn1-5* seeds were buried under 1 cm of sterile, sandy loamy soil. Seedlings were
494 scanned after 6 days post-sowing by X-Ray microcomputed tomography as described
495 previously (Orman-Ligeza, et al., 2018) at 6.5 μm resolution.

496 **References**

497 Abbas, M., Alabadi, D., and Blazquez, M.A. (2013). Differential growth at the apical hook: all roads
498 lead to auxin. Front Plant Sci 4.

499 Belteton, S.A., Sawchuk, M.G., Donohoe, B.S., Scarpella, E., and Szymanski, D.B. (2018).
500 Reassessing the Roles of PIN Proteins and Anticlinal Microtubules during Pavement Cell
501 Morphogenesis. Plant Physiol 176, 432-449.

502 Boudaoud, A., Burian, A., Borowska-Wykret, D., Uyttewaal, M., Wrzalik, R., Kwiatkowska, D., and
503 Hamant, O. (2014). FibrilTool, an ImageJ plug-in to quantify fibrillar structures in raw microscopy
504 images. Nat Protoc 9, 457-463.

505 Bouquin, T., Mattsson, O., Naested, H., Foster, R., and Mundy, J. (2003). The Arabidopsis lue1
506 mutant defines a katanin p60 ortholog involved in hormonal control of microtubule orientation
507 during cell growth. J Cell Sci 116, 791-801.

508 Boutte, Y., Jonsson, K., McFarlane, H.E., Johnson, E., Gendre, D., Swarup, R., Friml, J.,
509 Samuels, L., Robert, S., and Bhalerao, R.P. (2013). ECHIDNA-mediated post-Golgi trafficking of
510 auxin carriers for differential cell elongation. Proc Natl Acad Sci U S A 110, 16259-64.

511 Braam, J. (2005). In touch: plant responses to mechanical stimuli. New Phytol 165, 373-389.

512 Bringmann, M., Li, E.Y., Sampathkumar, A., Kocabek, T., Hauser, M.T., and Persson, S. (2012).
513 POM-POM2/CELLULOSE SYNTHASE INTERACTING1 Is Essential for the Functional
514 Association of Cellulose Synthase and Microtubules in Arabidopsis. Plant Cell 24, 163-177.

515 Burk, D.H., and Ye, Z.H. (2002). Alteration of oriented deposition of cellulose microfibrils by
516 mutation of a katanin-like microtubule-severing protein. Plant Cell 14, 2145-2160.

517 Cao, M., Chen, R., Li, P., Yu, Y.Q., Zheng, R., Ge, D.F., Zheng, W., Wang, X.H., Gu, Y.T., Gelova,
518 Z., et al. (2019). TMK1-mediated auxin signalling regulates differential growth of the apical hook.
519 Nature 568, 240-+.

520 Chaiwanon, J., Wang, W.F., Zhu, J.Y., Oh, E., and Wang, Z.Y. (2016). Information Integration
521 and Communication in Plant Growth Regulation. Cell 164, 1257-1268.

522 Chakrabortty, B., Blilou, I., Scheres, B., and Mulder, B.M. (2018). A computational framework for
523 cortical microtubule dynamics in realistically shaped plant cells. Plos Comput Biol 14.

524 Dai, N., Wang, W.Y., Patterson, S.E., and Bleecker, A.B. (2013). The TMK Subfamily of Receptor-
525 Like Kinases in Arabidopsis Display an Essential Role in Growth and a Reduced Sensitivity to
526 Auxin. Plos One 8.

527 DeBolt, S., Gutierrez, R., Ehrhardt, D.W., and Somerville, C. (2007). Nonmotile cellulose synthase
528 subunits repeatedly accumulate within localized regions at the plasma membrane in Arabidopsis
529 hypocotyl cells following 2,6-dichlorobenzonitrile treatment. Plant Physiol 145, 334-338.

530 Dixit, R., and Cyr, R. (2004). Encounters between dynamic cortical microtubules promote ordering
531 of the cortical array through angle-dependent modifications of microtubule behavior. Plant Cell
532 16, 3274-3284.

533 Echevin, E., Le Gloanec, C., Skowronska, N., Routier-Kierzkowska, A.L., Burian, A., and
534 Kierzkowski, D. (2019). Growth and biomechanics of shoot organs. J Exp Bot 70, 3573-3585.

535 Erguvan, O., Louveaux, M., Hamant, O., and Verger, S. (2019). ImageJ SurfCut: a user-friendly
536 pipeline for high-throughput extraction of cell contours from 3D image stacks. Bmc Biol 17.

537 Farge, E. (2003). Mechanical induction of twist in the Drosophila foregut/stomodeal primordium.
538 Current Biology 13, 1365-1377.

539 Feraru, E., Feraru, M.I., Kleine-Vehn, J., Martiniere, A., Mouille, G., Vanneste, S., Vernhettes, S.,
540 Runions, J., and Friml, J. (2011). PIN Polarity Maintenance by the Cell Wall in Arabidopsis.
541 Current Biology 21, 338-343.

542 Franck, A.D., Powers, A.F., Gestaut, D.R., Gonen, T., Davis, T.N., and Asbury, C.L. (2007).
543 Tension applied through the Dam1 complex promotes microtubule elongation providing a direct
544 mechanism for length control in mitosis. Nat Cell Biol 9, 832-U171.

545 Fujita, M., Himmelspach, R., Ward, J., Whittington, A., Hasenbein, N., Liu, C., Truong, T.T.,
546 Galway, M.E., Mansfield, S.D., Hocart, C.H., et al. (2013). The anisotropy1 D604N Mutation in
547 the Arabidopsis Cellulose Synthase1 Catalytic Domain Reduces Cell Wall Crystallinity and the
548 Velocity of Cellulose Synthase Complexes. Plant Physiol 162, 74-85.

549 Grunewald, W., and Friml, J. (2010). The march of the PINs: developmental plasticity by dynamic
550 polar targeting in plant cells. Embo J 29, 2700-2714.

551 Hamant, O., and Haswell, E.S. (2017). Life behind the wall: sensing mechanical cues in plants.
552 Bmc Biol 15.

553 Hamant, O., Heisler, M.G., Jonsson, H., Krupinski, P., Uyttewaal, M., Bokov, P., Corson, F.,
554 Sahlin, P., Boudaoud, A., Meyerowitz, E.M., et al. (2008). Developmental Patterning by
555 Mechanical Signals in Arabidopsis. Science 322, 1650-1655.

556 Hamant, O., Inoue, D., Bouchez, D., Dumais, J., and Mjolsness, E. (2019). Are microtubules
557 tension sensors? Nat Commun 10.

558 Heisler, M.G., Hamant, O., Krupinski, P., Uyttewaal, M., Ohno, C., Jonsson, H., Traas, J., and
559 Meyerowitz, E.M. (2010). Alignment between PIN1 Polarity and Microtubule Orientation in the
560 Shoot Apical Meristem Reveals a Tight Coupling between Morphogenesis and Auxin Transport.
561 Plos Biol 8.

562 Heisler, M.G., Ohno, C., Das, P., Sieber, P., Reddy, G.V., Long, J.A., and Meyerowitz, E.M.
563 (2005). Patterns of auxin transport and gene expression during primordium development revealed
564 by live imaging of the Arabidopsis inflorescence meristem. Current Biology 15, 1899-1911.

565 Hervieux, N., Tsugawa, S., Fruleux, A., Dumond, M., Routier-Kierzkowska, A.L., Komatsuzaki,
566 T., Boudaoud, A., Larkin, J.C., Smith, R.S., Li, C.B., et al. (2017). Mechanical Shielding of Rapidly
567 Growing Cells Buffers Growth Heterogeneity and Contributes to Organ Shape Reproducibility.
568 Current Biology 27, 3468-+.

569 Huang, C.J., Wang, Z.L., Quinn, D., Suresh, S., and Hsia, K.J. (2018). Differential growth and
570 shape formation in plant organs. P Natl Acad Sci USA 115, 12359-12364.

571 Ikushima, T., and Shimmen, T. (2005). Mechano-sensitive orientation of cortical microtubules
572 during gravitropism in azuki bean epicotyls. J Plant Res 118, 19-26.

573 Inoue, D., Nitta, T., Kabir, A.M.R., Sada, K., Gong, J.P., Konagaya, A., and Kakugo, A. (2016).
574 Sensing surface mechanical deformation using active probes driven by motor proteins. Nat
575 Commun 7.

576 Ishida, T., Kaneko, Y., Iwano, M., and Hashimoto, T. (2007). Helical microtubule arrays in a
577 collection of twisting tubulin mutants of Arabidopsis thaliana. P Natl Acad Sci USA 104, 8544-
578 8549.

579 Kutschera, U., and Nikas, K.J. (2007). The epidermal-growth-control theory of stem elongation:
580 An old and a new perspective. J Plant Physiol 164, 1395-1409.

581 Landrein, B., Kiss, A., Sassi, M., Chauvet, A., Das, P., Cortizo, M., Laufs, P., Takeda, S., Aida,
582 M., Traas, J., et al. (2015). Mechanical stress contributes to the expression of the STM homeobox
583 gene in Arabidopsis shoot meristems. Elife 4.

584 Li, T., Yan, A., Bhatia, N., Altinok, A., Afik, E., Durand-Smet, P., Tarr, P.T., Schroeder, J.I., Heisler,
585 M.G., and Meyerowitz, E.M. (2019). Calcium signals are necessary to establish auxin transporter
586 polarity in a plant stem cell niche. Nat Commun 10.

587 Lin, D., Cao, L., Zhou, Z., Zhu, L., Ehrhardt, D., Yang, Z., and Fu, Y. (2013). Rho GTPase
588 signaling activates microtubule severing to promote microtubule ordering in Arabidopsis. Curr Biol
589 23, 290-7.

590 Louveaux, M., Rochette, S., Beauzamy, L., Boudaoud, A., and Hamant, O. (2016). The impact of
591 mechanical compression on cortical microtubules in Arabidopsis: a quantitative pipeline. Plant J
592 88, 328-342.

593 Luptovciak, I., Komis, G., Takac, T., Ovecka, M., and Samaj, J. (2017). Katanin: A Sword Cutting
594 Microtubules for Cellular, Developmental, and Physiological Purposes. Front Plant Sci 8.

595 Marc, J., Granger, C.L., Brincat, J., Fisher, D.D., Kao, T.H., McCubbin, A.G., and Cyr, R.J. (1998).
596 A GFP-MAP4 reporter gene for visualizing cortical microtubule rearrangements in living epidermal
597 cells. Plant Cell 10, 1927-1939.

598 Martin, A.C., Kaschube, M., and Wieschaus, E.F. (2009). Pulsed contractions of an actin-myosin
599 network drive apical constriction. Nature 457, 495-U11.

600 Mazzella, M.A., Casal, J.J., Muschietti, J.P., and Fox, A.R. (2014). Hormonal networks involved
601 in apical hook development in darkness and their response to light. Front Plant Sci 5.

602 Nakayama, N., Smith, R.S., Mandel, T., Robinson, S., Kimura, S., Boudaoud, A., and Kuhlemeier,
603 C. (2012). Mechanical Regulation of Auxin-Mediated Growth. Current Biology 22, 1468-1476.

604 Okushima, Y., Overvoorde, P.J., Arima, K., Alonso, J.M., Chan, A., Chang, C., Ecker, J.R.,
605 Hughes, B., Lui, A., Nguyen, D., et al. (2005). Functional genomic analysis of the AUXIN
606 RESPONSE FACTOR gene family members in Arabidopsis thaliana: Unique and overlapping
607 functions of ARF7 and ARF19. Plant Cell 17, 444-463.

608 Orman-Ligeza, B., Morris, E.C., Parizot, B., Lavigne, T., Babe, A., Ligeza, A., Klein, S., Sturrock,
609 C., Xuan, W., Novak, O., et al. (2018). The Xerobranching Response Represses Lateral Root
610 Formation When Roots Are Not in Contact with Water. Current Biology 28, 3165-+.

611 Paredez, A.R., Somerville, C.R., and Ehrhardt, D.W. (2006). Visualization of cellulose synthase
612 demonstrates functional association with microtubules. Science 312, 1491-1495.

613 Pouille, P.A., Ahmadi, P., Brunet, A.C., and Farge, E. (2009). Mechanical Signals Trigger Myosin
614 II Redistribution and Mesoderm Invagination in Drosophila Embryos. Sci Signal 2.

615 Raz, V., and Koornneef, M. (2001). Cell division activity during apical hook development. Plant
616 Physiol 125, 219-226.

617 Risca, V.I., Wang, E.B., Chaudhuri, O., Chia, J.J., Geissler, P.L., and Fletcher, D.A. (2012). Actin
618 filament curvature biases branching direction. P Natl Acad Sci USA 109, 2913-2918.

619 Robinson, S., and Kuhlemeier, C. (2018). Global Compression Reorients Cortical Microtubules in
620 Arabidopsis Hypocotyl Epidermis and Promotes Growth. Current Biology 28, 1794-+.

621 Sampathkumar, A., Krupinski, P., Wightman, R., Milani, P., Berquand, A., Boudaoud, A., Hamant,
622 O., Jonsson, H., and Meyerowitz, E.M. (2014). Subcellular and supracellular mechanical stress
623 prescribes cytoskeleton behavior in Arabidopsis cotyledon pavement cells. Elife 3.

624 Sherrard, K., Robin, F., Lemaire, P., and Munro, E. (2010). Sequential Activation of Apical and
625 Basolateral Contractility Drives Ascidian Endoderm Invagination. Current Biology 20, 1499-1510.

626 Trushko, A., Schaffer, E., and Howard, J. (2013). The growth speed of microtubules with
627 XMAP215-coated beads coupled to their ends is increased by tensile force. P Natl Acad Sci USA
628 110, 14670-14675.

629 Uyttewaal, M., Burian, A., Alim, K., Landrein, B.T., Borowska-Wykret, D., Dedieu, A., Peaucelle,
630 A., Ludynia, M., Traas, J., Boudaoud, A., et al. (2012). Mechanical Stress Acts via Katanin to
631 Amplify Differences in Growth Rate between Adjacent Cells in Arabidopsis. Cell 149, 439-451.

632 Vandenbussche, F., Petrasek, J., Zadnikova, P., Hoyerova, K., Pesek, B., Raz, V., Swarup, R.,
633 Bennett, M., Zazimalova, E., Benkova, E., et al. (2010). The auxin influx carriers AUX1 and LAX3
634 are involved in auxin-ethylene interactions during apical hook development in Arabidopsis
635 thaliana seedlings. Development 137, 597-606.

636 Yu, M., Yuan, X., Lu, C., Le, S.M., Kawamura, R., Efremov, A.K., Zhao, Z.H., Kozlov, M.M.,
637 Sheetz, M., Bershadsky, A., et al. (2017). mDia1 senses both force and torque during F-actin
638 filament polymerization. Nat Commun 8.

639 Zadnikova, P., Petrasek, J., Marhavy, P., Raz, V., Vandenbussche, F., Ding, Z.J., Schwarzerova,
640 K., Morita, M.T., Tasaka, M., Hejatko, J., et al. (2010). Role of PIN-mediated auxin efflux in apical
641 hook development of Arabidopsis thaliana. Development 137, 607-617.

642 Zadnikova, P., Wabnik, K., Abuzeineh, A., Gallemi, M., Van Der Straeten, D., Smith, R.S., Inze,
643 D., Friml, J., Prusinkiewicz, P., and Benkova, E. (2016). A Model of Differential Growth-Guided
644 Apical Hook Formation in Plants. Plant Cell 28, 2464-2477.

Zhu, Q., Gallemi, M., Pospisil, J., Zadnikova, P., Strnad, M., and Benkova, E. (2019). Root gravity response module guides differential growth determining both root bending and apical hook formation in Arabidopsis. Development 146.

Figure

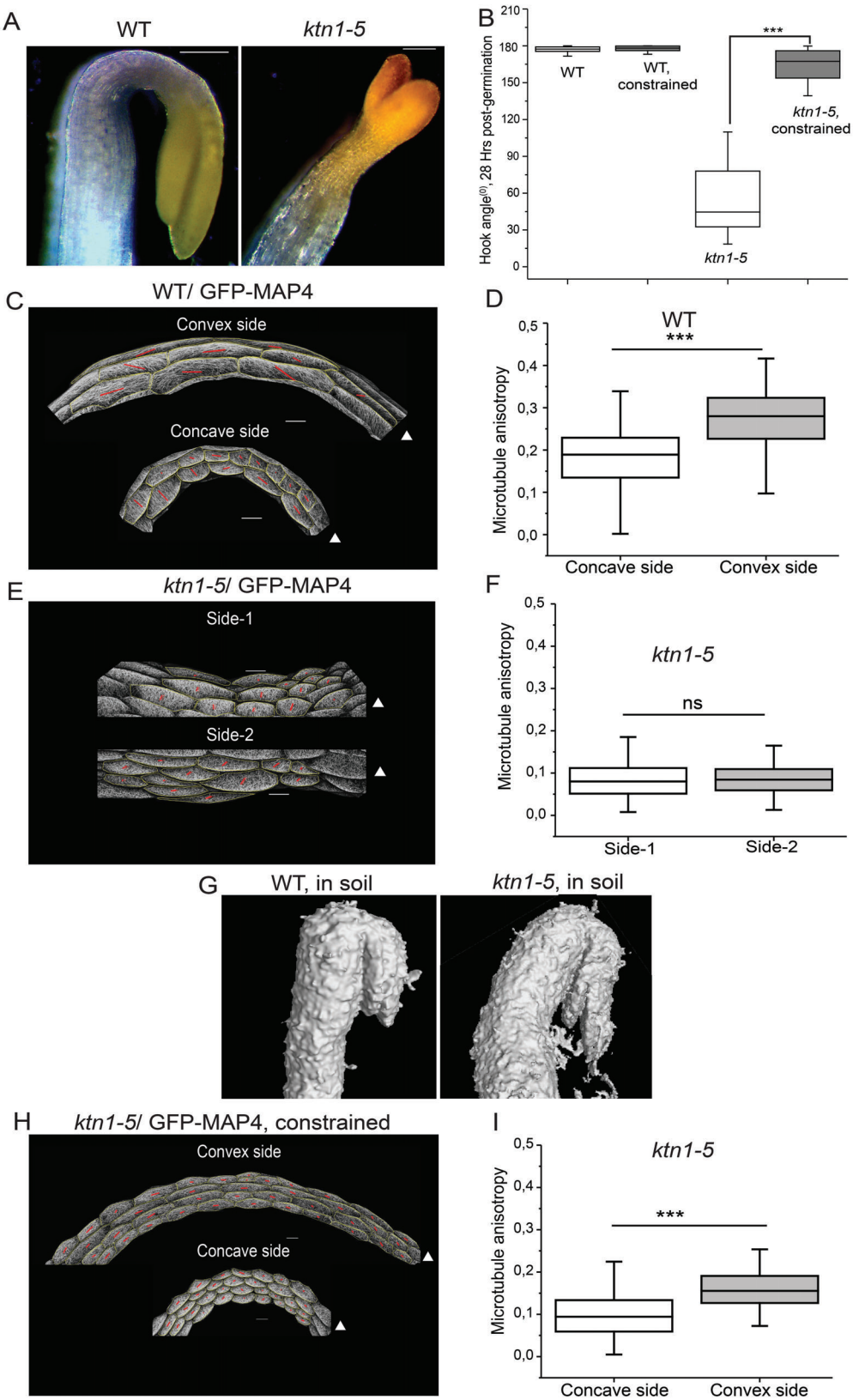

Figure. 1 *ktn1-5* mutant has a strong apical hook defect, which can be rectified by mechanical constrain of soil.

(A) Representative image of WT and *ktn1-5* seedling grown without mechanical constrain 30 Hrs after germination. (B) Quantification of apical-hook angles in WT and *ktn1-5* seedlings growing on the surface of MS agar or growing through the gel (constrained), 28 Hrs after germination, n = 20 seedlings. (C-F) CMT organization in the hook region (0-400 µm from the shoot apical meristem) of WT, and *ktn1-5* seedlings.Representative image of CMTs visualized with GFP-MAP4 (C, E). The length of the red lines in each cell represent the average CMT anisotropy of the cell quantified by Fibriltool. Triangles denote the end of the hypocotyl with the shoot apical meristem. Quantification of CMT anisotropy values (D, F) across two sides of the hypocotyl measured by FibrilTool. Anisotropy values from at least 150 cells from 5 seedlings were quantified per group. (G) Representative image of soil embedded WT and *ktn1-5* seedling. Seeds were buried under 1 cm of sandy loamy soil and imaged by micro CT, 6 days after sowing. (H-I) CMT organization in the hook region of *ktn1-5* seedlings grown in presence of mechanical constrain (inside agar); representative image (H) and anisotropy calculation using Fibriltool (I). The data in C, D, F, and I are plotted as box plots showing the first and third quartiles, split by the median; whiskers extended to minimum and maximum values. Asterisks (***) indicate P < 0.0001 (Student's two tailed t-test). Scale bar = 200 µm in A and 20 µm in D, E, F.

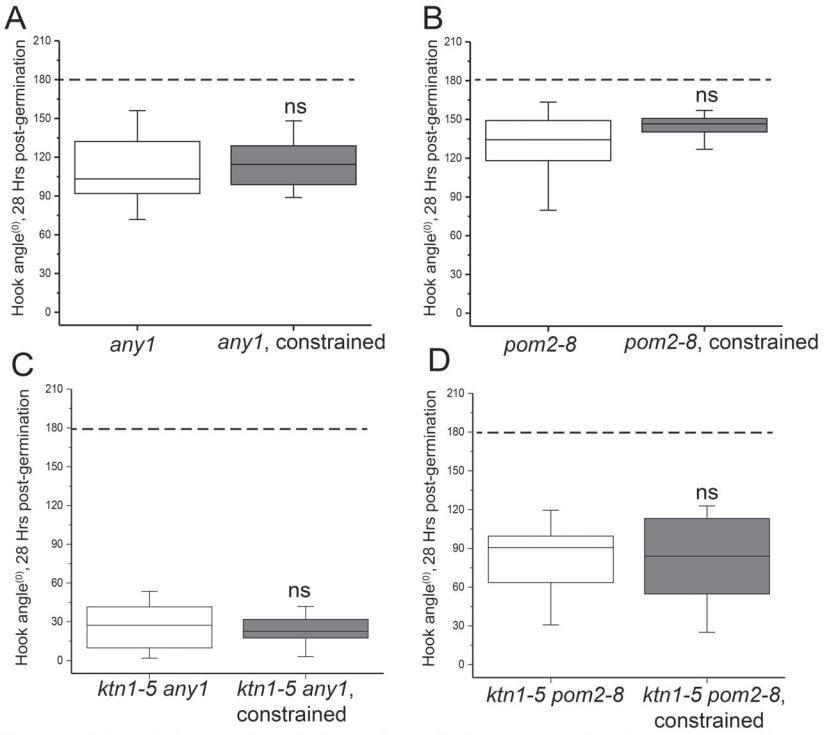

Figure. 2 Hook formation defects in cellulose organization mutants is not rectified by mechanical constrain.

Quantification of apical-hook angles in *any1* (A) and *pom2-8* seedlings (B) growing on the surface of MS agar or growing through the gel (constrained), 28 Hrs after germination, n = 20 seedlings. (C-D) Quantification of apical hook angles in *ktn1-5 any1* (C) and *ktn1-5 pom2-8* (D) double mutant seedlings. 28 Hrs after germination, n = 16 seedlings. The data in is plotted as box plots showing the first and third quartiles, split by the median; whiskers extended to minimum and maximum values. The dashed line denotes hook angle of 180^0. ns = non-significant at $P \leq 0.05$ (Student's two tailed t-test).

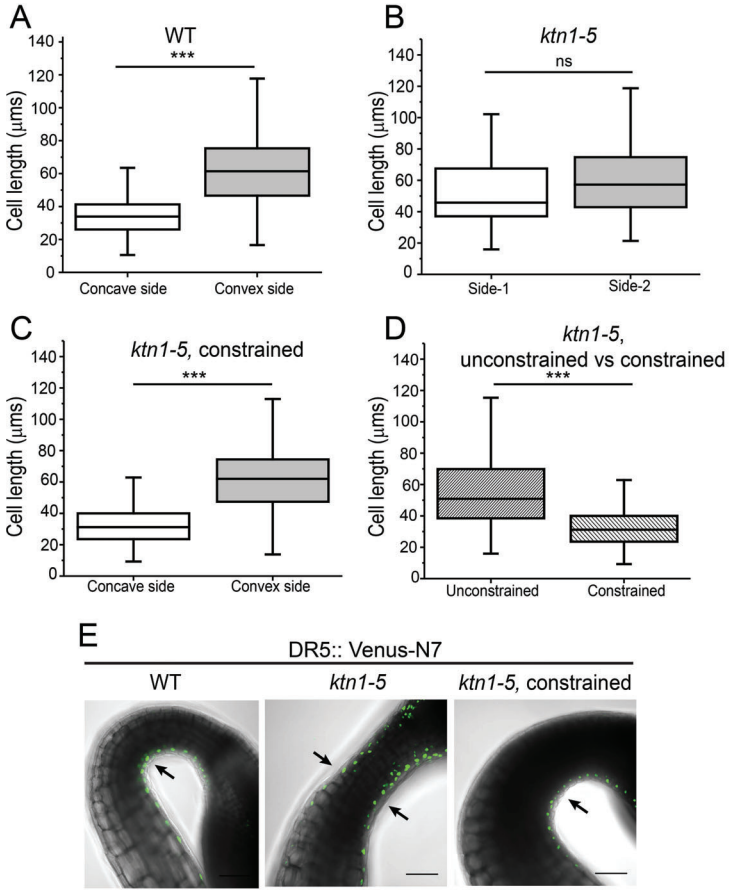

Figure. 3 Mechanical constrain reestablishes auxin response maxima and cell length repression in *ktn1-5* seedlings.

(A-C) Quantification of cell length of WT (A), *ktn1-5* (B) and mechanically constrained *ktn1-5* seedlings (C) in the hook region (0-400 µm from the shoot apical meristem). Cell length is measured from at least 150 cells from 5 seedlings per group, where cell outlines were marked with GFP-MAP4.
(D) Comparison of average cell length in the hook region of unconstrained *ktn1-5* seedlings with concave side cells constrained *ktn1-5* seedlings shows cell growth repression reestablishment by mechanical constrain. Box plots show the first and third quartiles, split by the median; whiskers extended to minimum and maximum values. Asterisks (***) indicate $P < 0.0001$, ns = non-significant at $P \leq 0.05$ (Student's two tailed t-test). (E) Representative image of DR5:: Venus-N7 signal in WT and *ktn1-5* seedlings, 28-30 Hrs post germination. In WT, DR5:: Venus-N7 signal is detected only in epidermal cells on the concave side of apical hook (arrow). In *ktn1-5*, DR5::Venus-N7 signal is seen on both sides of the hypocotyl (arrows) suggesting a defect in auxin asymmetry establishment. DR5::Venus-N7 signal asymmetry is reestablished in *ktn1-5* by mechanical constrain by growing inside agar. Scale bar = 100 µm.

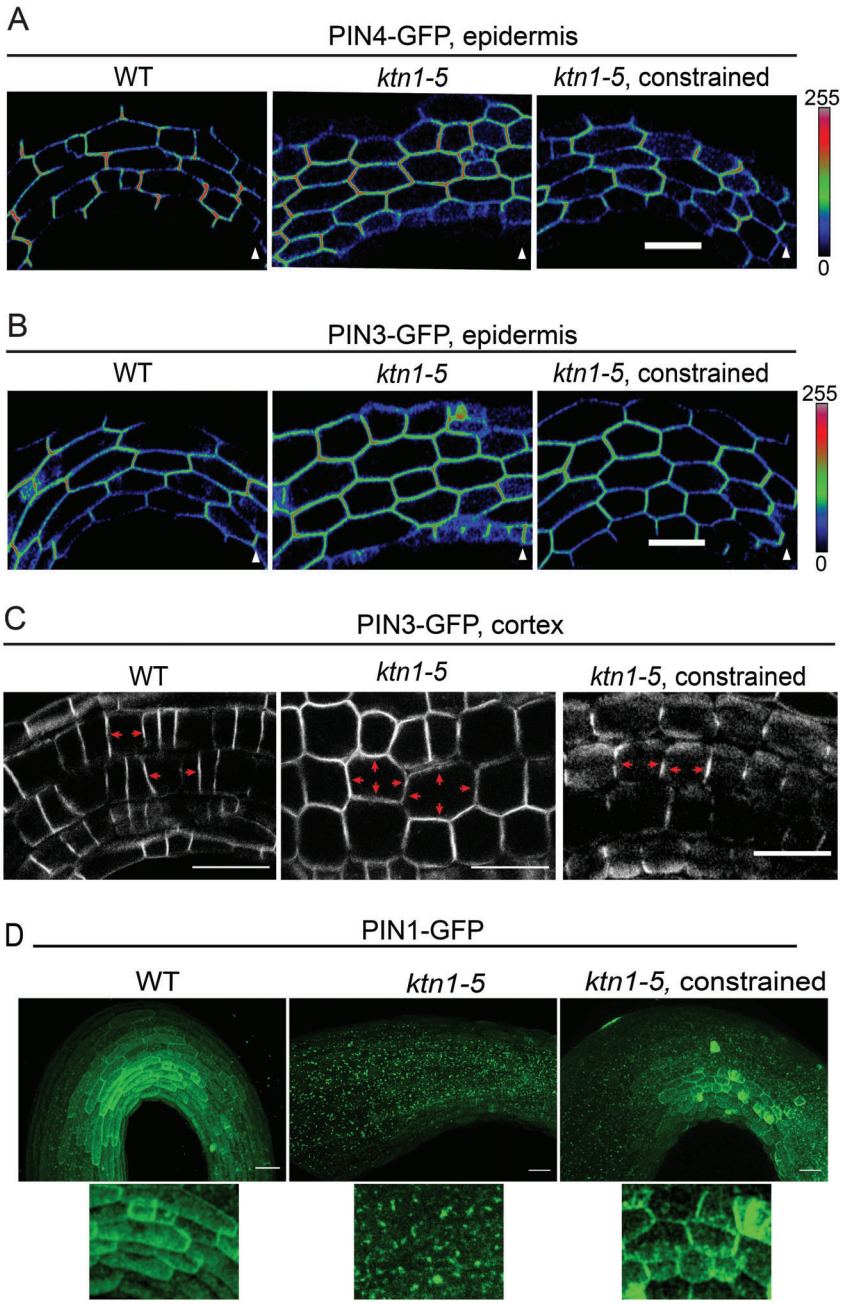

Figure. 4 Altered localization of PIN auxin transporters in *ktn1-5* could be rectified by mechanical constrain.

Representative images of PIN4-GFP in epidermis (A), PIN3-GFP in epidermis (B) and PIN3-GFP in cortex (C) in WT, *ktn1-5* and mechanically constrained *ktn1-5* seedlings. (D) PIN1-GFP in WT hook (left) shows plasma membrane localization only on concave side of the hook. In *ktn1-5* seedlings PIN1-GFP is absent from the plasma membrane (middle). In mechanically constrained *ktn1-5* seedlings, PIN1-GFP is seen on plasma membrane on cells on concave side (right). Magnified images of concave side cells are shown underneath. Scale bar = 50 µm. Color bars in (A) and (B) represent 8-bit intensity range of 0-255, triangles denote the end of the hypocotyl with the shoot apical meristem. See also **Figure.S5**.

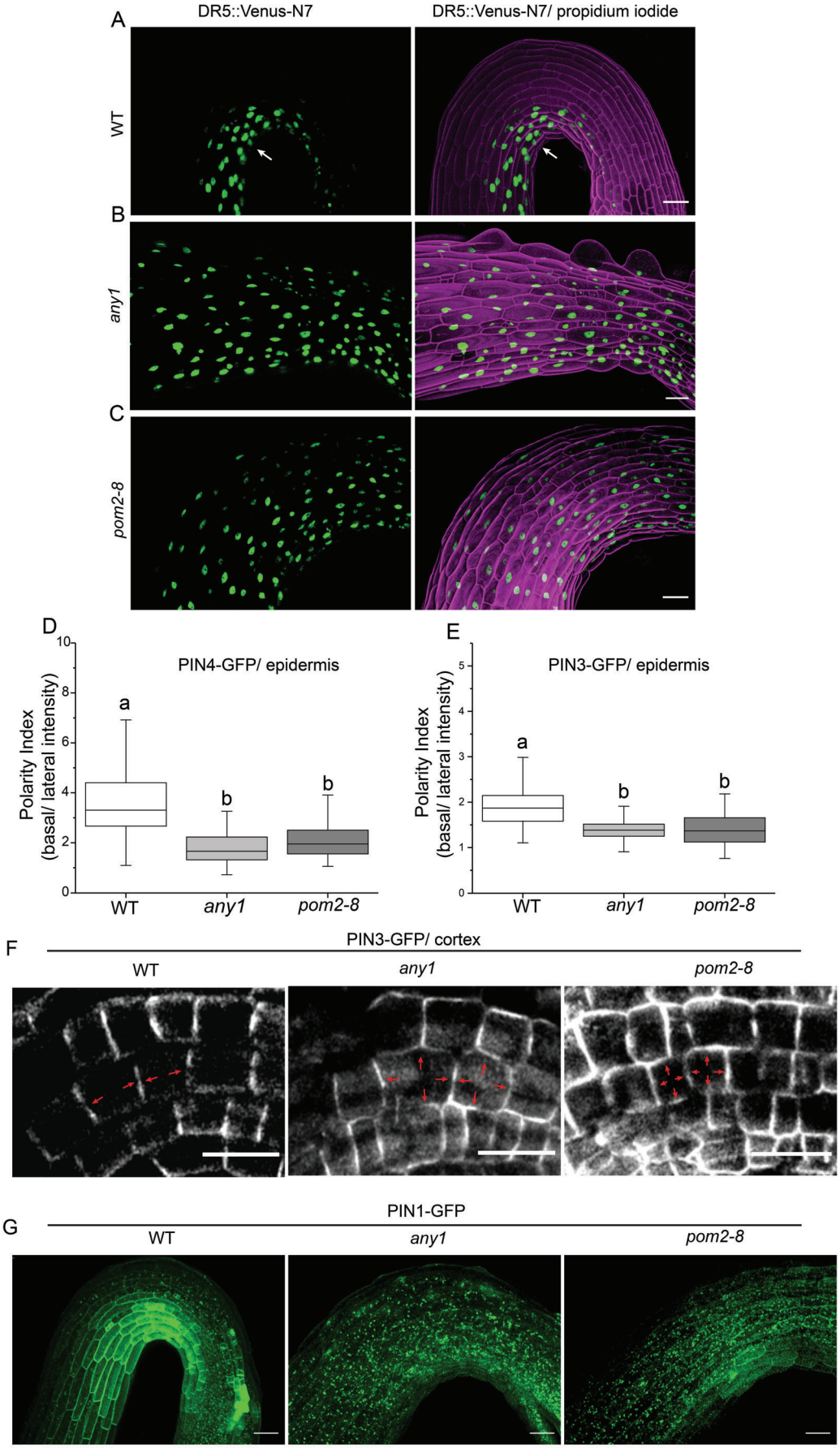

Figure. 5 Altered auxin response asymmetry and PIN localization in cellulose mutants

(A-C) Representative image showing Z-projection of DR5:: Venus-N7 signal in WT (A), *any1* (B) and *pom2-8* (C) seedlings. The cells are counterstained with propidium iodide. The concave side specific localization of DR5::Venus-N7 signal seen in WT (arrow) is altered in *any1* and *pom2-8* Scale bar = 50 µm. (D-E) Quantification of polarity index (basal/ lateral fluorescence intensity) of PIN4-GFP (D) and PIN3-GFP (E) in epidermal cells of hook region of WT, *any1* and *pom2-8* seedlings. Polarity index was measured from at least 100 cells from 10 seedlings/ group. Box plots show the first and third quartiles, split by the median; whiskers extended to minimum and maximum values. Groups with significant difference by one-way ANOVA with post hoc Tukey's test ($P < 0.05$) are indicated by different letters. (F) Representative images showing localization of PIN3-GFP in hook region cortical cells of WT, *any1* and *pom2-8* seedlings. (G) Localization of PIN1-GFP in WT, *any1* and *pom2-8* seedlings. Scale bar = 50µm. See also **Figure. S6**.

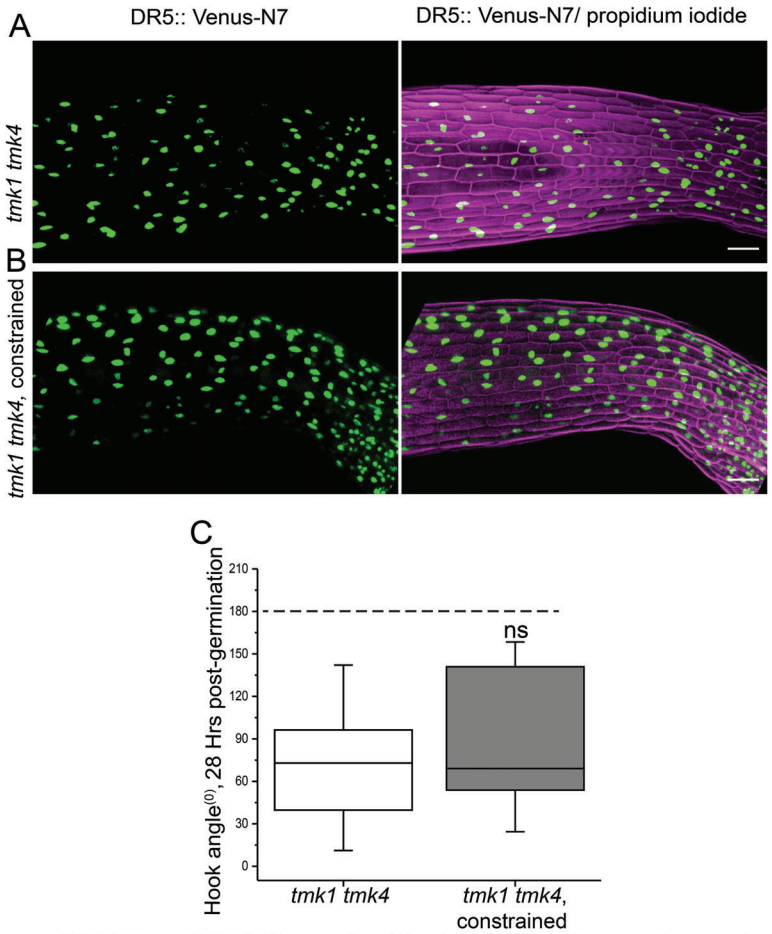

Figure. 6 TMK1 and TMK4 is required for hook formation under mechanical constrain

Representative image showing Z-projection of DR5::Venus-N7 signal in *tmk1 tmk4* seedling in absence (A) and in presence of mechanical constrain (B). The cells are counterstained with propidium iodide, Scale bar = 50 µm. (C) Quantification of apical-hook angles in *tmk1 tmk4* growing on the surface of MS agar or growing through the gel (constrained), 28 Hrs after germination, n = 16 seedlings. Box plots show the first and third quartiles, split by the median; whiskers extended to minimum and maximum values. The dashed line denotes hook angle of 180^0. ns = non-significant at $P \leq 0.05$ (Student's two tailed t-test).

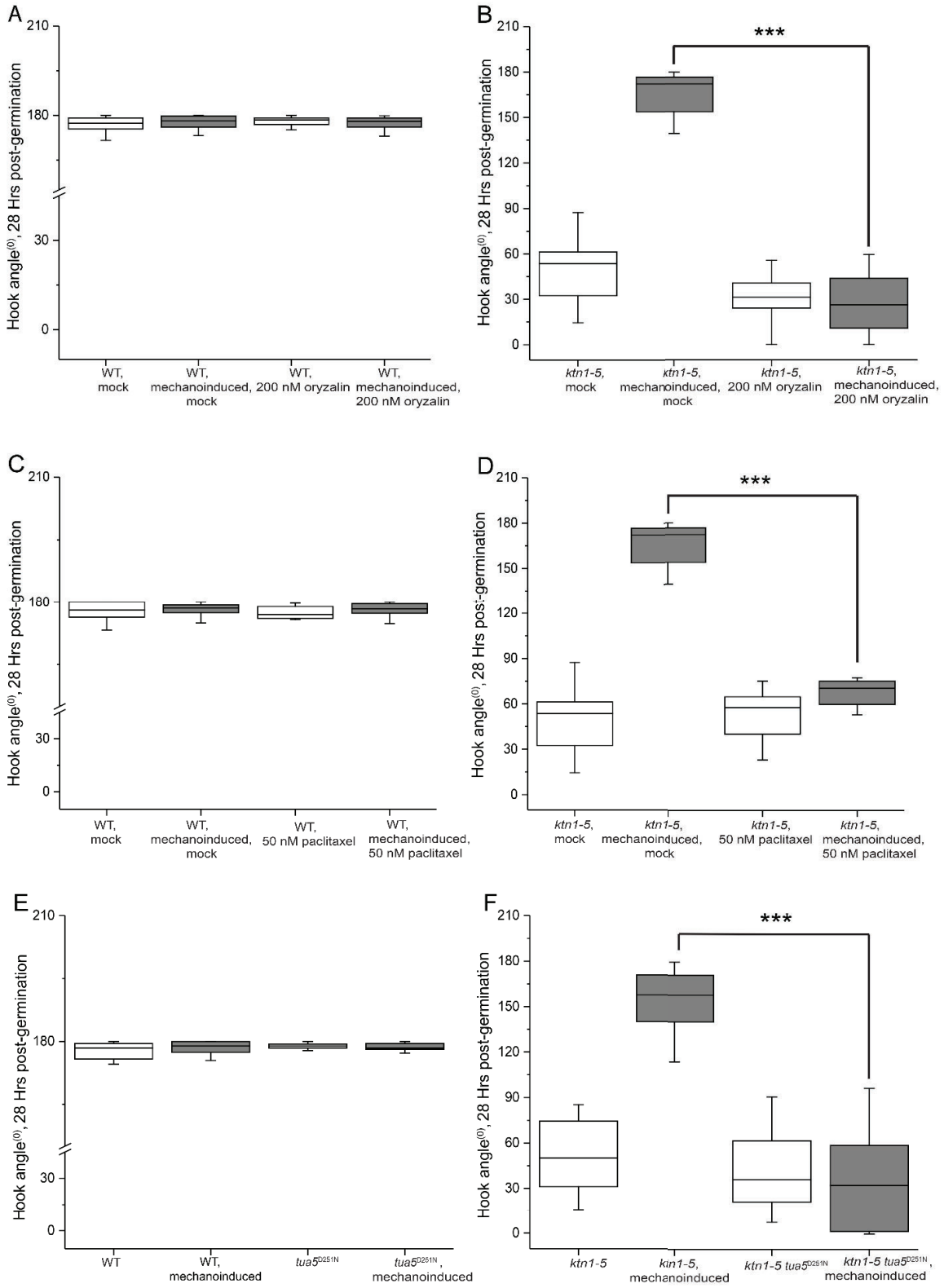

Figure. S1 Chemical and genetic perturbations of microtubules eliminate mechanically-constrained hook formation in the *ktn1-5* mutant. Quantification of apical hook angles in WT and *ktn1-5* seedlings (in the presence and absence of mechanical constraint) treated with 200 nM oryzalin (A, B) or 50 nM paclitaxel (C, D) or in the presence of the *tua5*^{D251N} mutation (E, F), 28 Hrs post-germination. n = 18 seedlings per group, box plots showing the first and third quartiles, split by the median; whiskers extend to minimum and maximum values. Indicated groups are compared by Student's two tailed t-test, asterisks (***) indicate P < 0.0001.

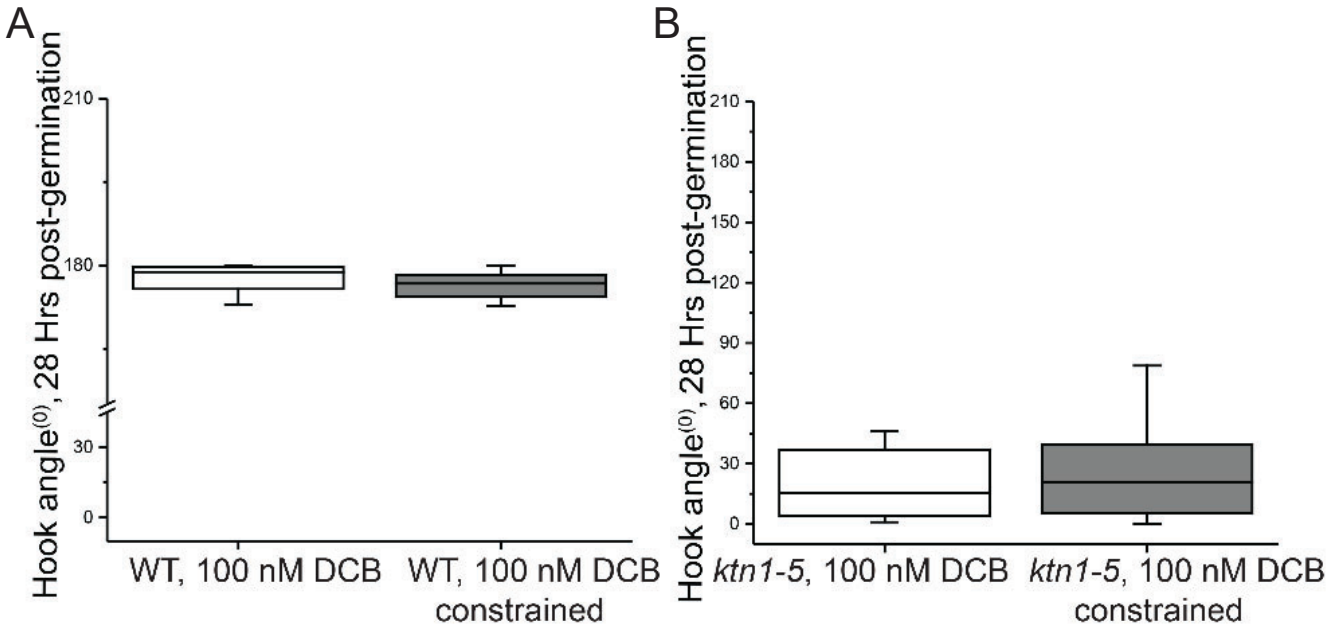

Figure. S2 Mechanically constrained hook formation in *ktn1-5* is hypersensitive to the cellulose biosynthesis inhibitor DCB. Quantification of apical-hook angles in WT (A) and *ktn1-5* (B) treated with 100 nM DCB in the absence or presence of mechanical constraint, 28 Hrs after germination. n = 16 seedlings/ group.

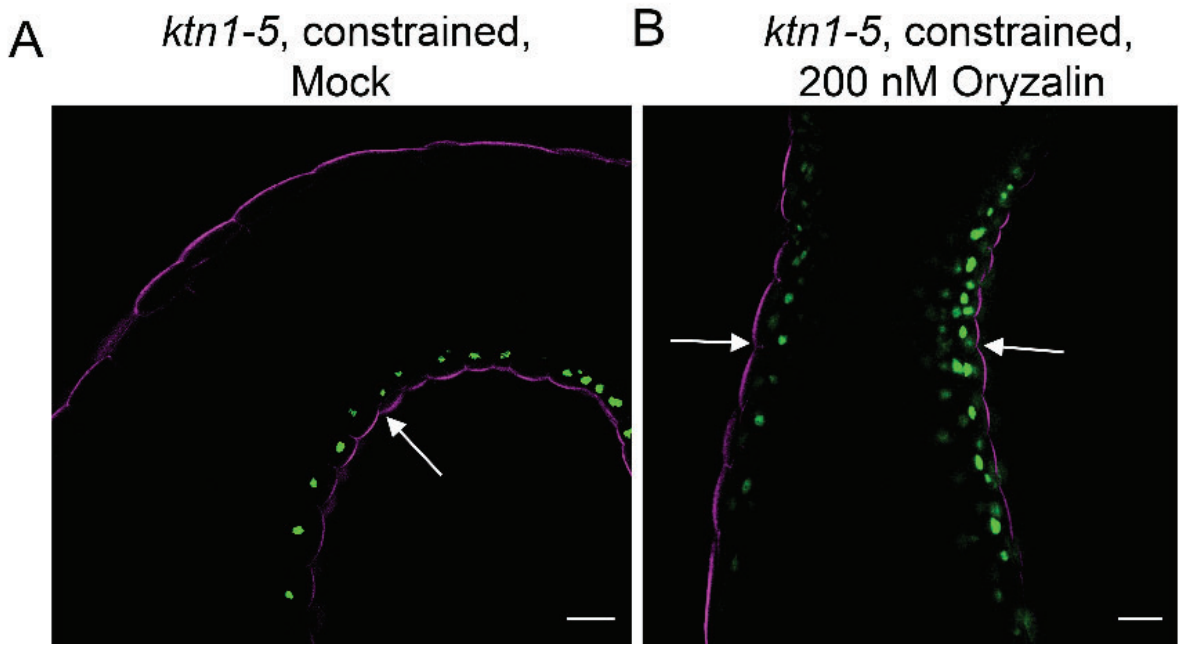

Figure. S3 Representative image of DR5:: Venus-N7 signal in mechanically constrained *ktn1-5* seedlings grown inside mock MS agar (A) or MS agar supplemented with 200 nM Oryzalin (B). The seedlings are counterstained with propidium iodide. DR5:: Venus-N7 signal is indicated by arrows. At least 10 seedlings were observed per group.

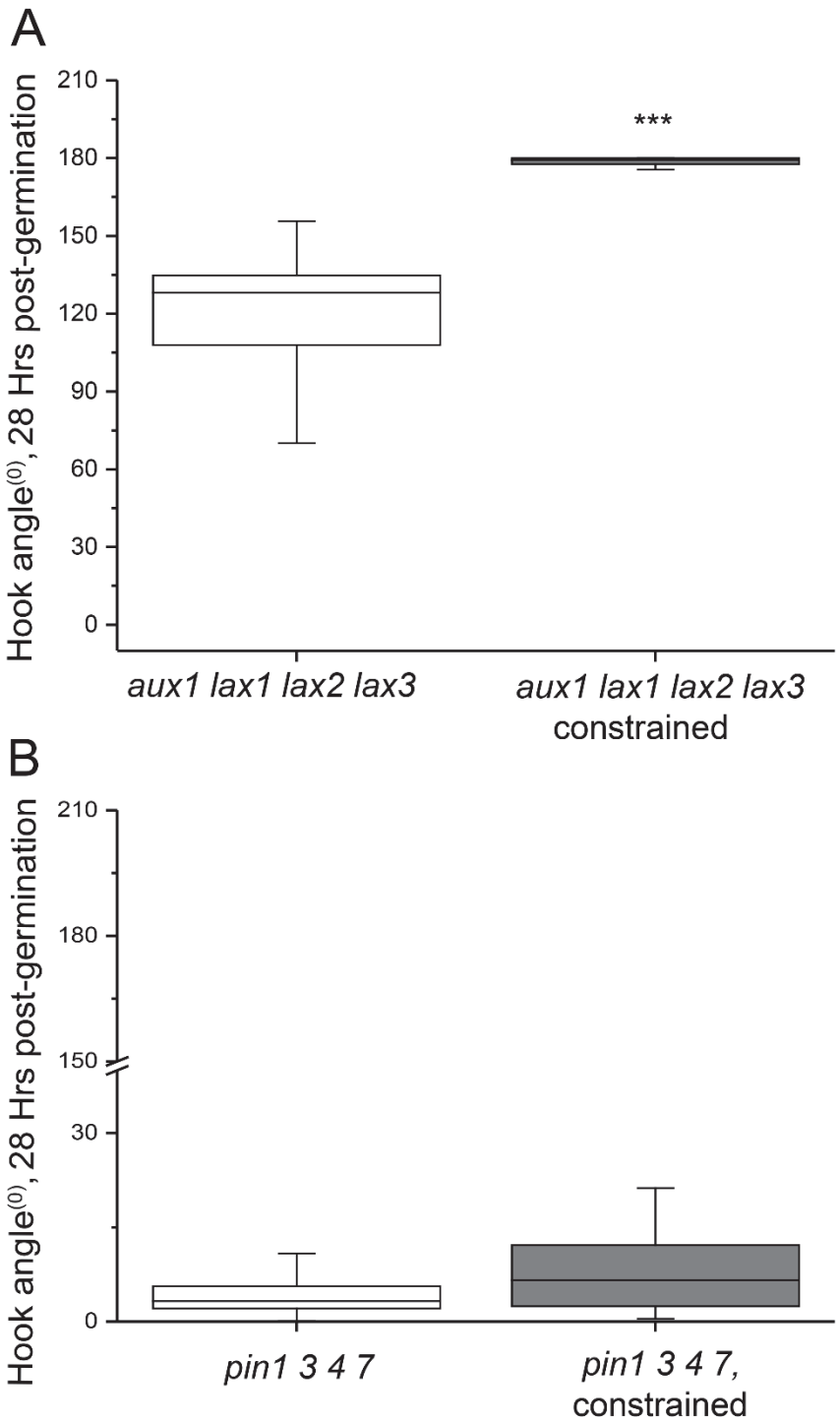

Figure. S4 Involvement of auxin carriers in mechanically constrained hook formation. Quantification of apical-hook angles in *aux1 lax1 lax2 lax3* quadruple mutant (A) and *pin1 3 4 7* quadruple mutant (B) growing on the surface of MS agar or growing through the gel (constrained), 28 Hrs after germination, n = 16 seedlings/ group. Box plots showing the first and third quartiles, split by the median; whiskers extend to minimum and maximum values. Indicated groups are compared by Student's two tailed t-test, asterisks (***) indicate $P < 0.0001$.

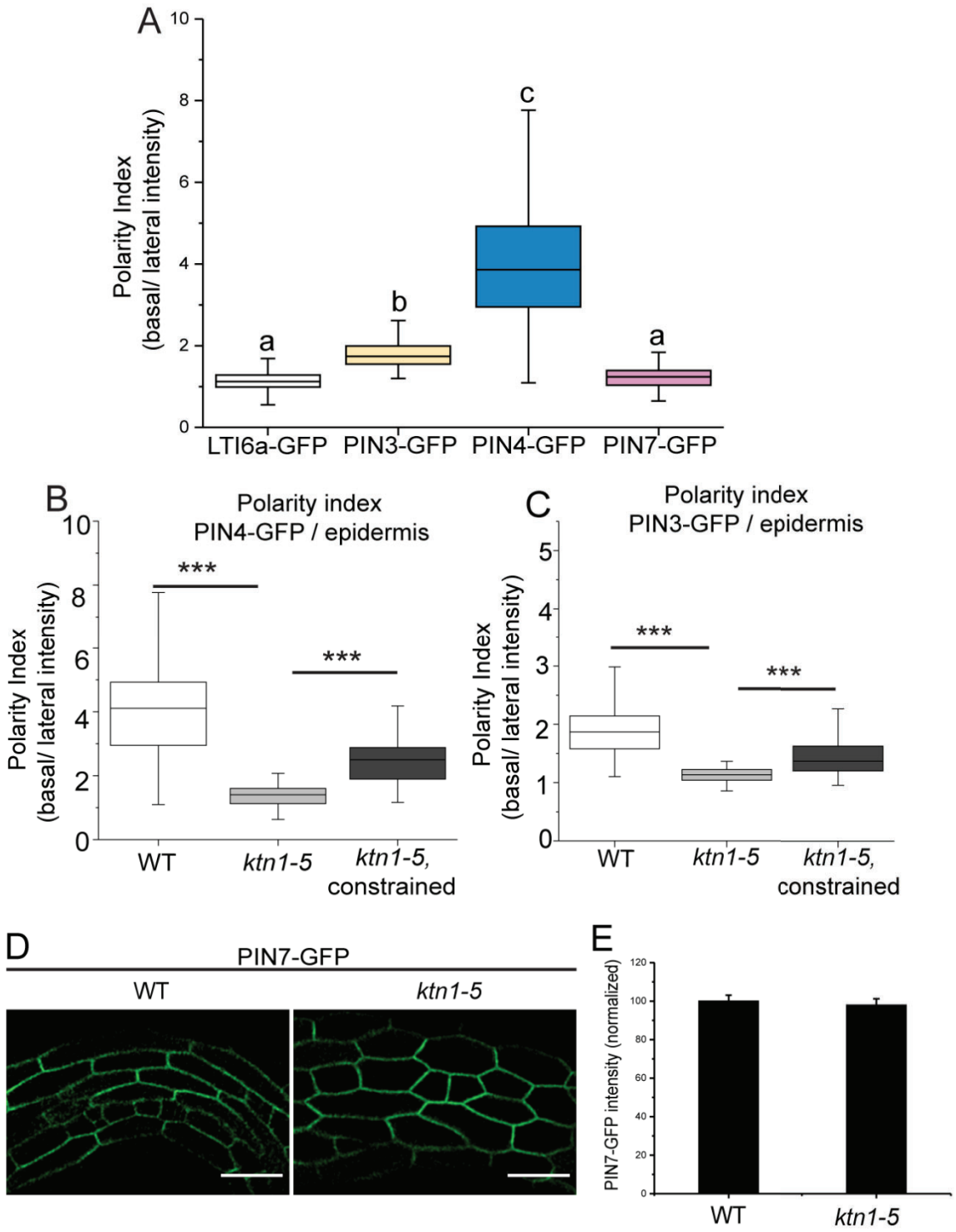

Figure. S5 Polarity of auxin transporters. (A) Quantification of polarity index (basal/ lateral fluorescence intensity) of PIN3-GFP, PIN4-GFP, PIN7-GFP and LTI6a-GFP in hook epidermal cells. Polarity index was measured from at least 100 cells from 10 seedlings/ group. Polarity of PINs are compared with the nonpolar localization of LTI6a-GFP by one-way ANOVA with Tukey's post-hoc test. Groups with significant difference ($P < 0.05$) are indicated by different letters. (B) Quantification of polarity index (basal/ lateral fluorescence intensity) of PIN4-GFP (A) and PIN3-GFP (B) in epidermal cells (related to Figure. 4A and 4B). Polarity index was measured from at least 100 cells from 10 seedlings/ group. Box plots show the first and third quartiles, split by the median; whiskers extended to minimum and maximum values. Asterisks (***) indicate $P < 0.0001$, ns = non-significant at $P \leq 0.05$ (Student's two tailed t-test). (C) Localization of PIN7-GFP in WT and ktn1-5 hook region. (D) quantification of PIN7-GFP intensities in WT and ktn1-5 hook. At least 100 cells from 10 seedlings per group was measured. Bars represent normalized mean ± S.E.M, ns = non-significant at $P \leq 0.05$ (Student's two tailed t-test).

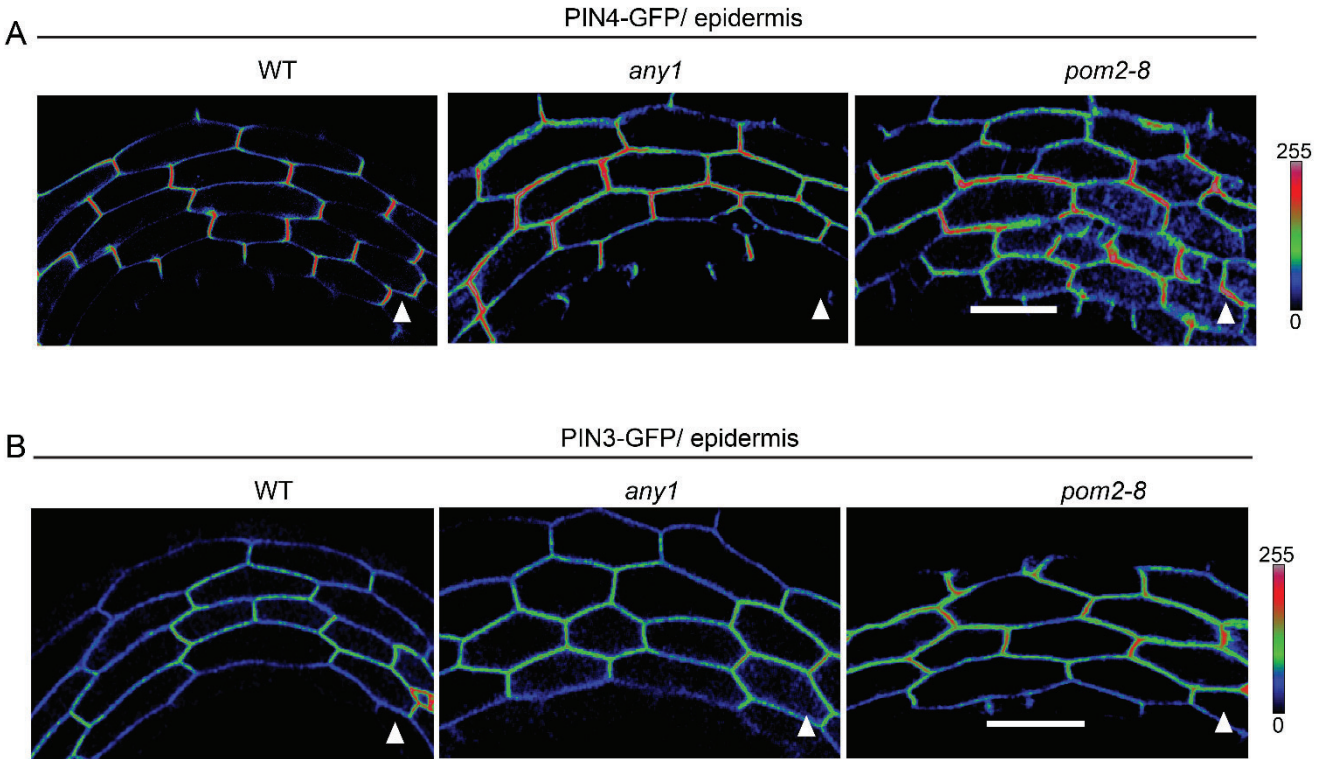

Figure. S6 Representative images of PIN4-GFP (A), PIN3-GFP (B) in epidermal cells of WT, *any1* and *pom2-8* apical hook. Triangles denote the end of the hypocotyl with the shoot apical meristem. Scale bar = 50 μm. Color bars in (A) and (B) represent 8-bit intensity range of 0-255.

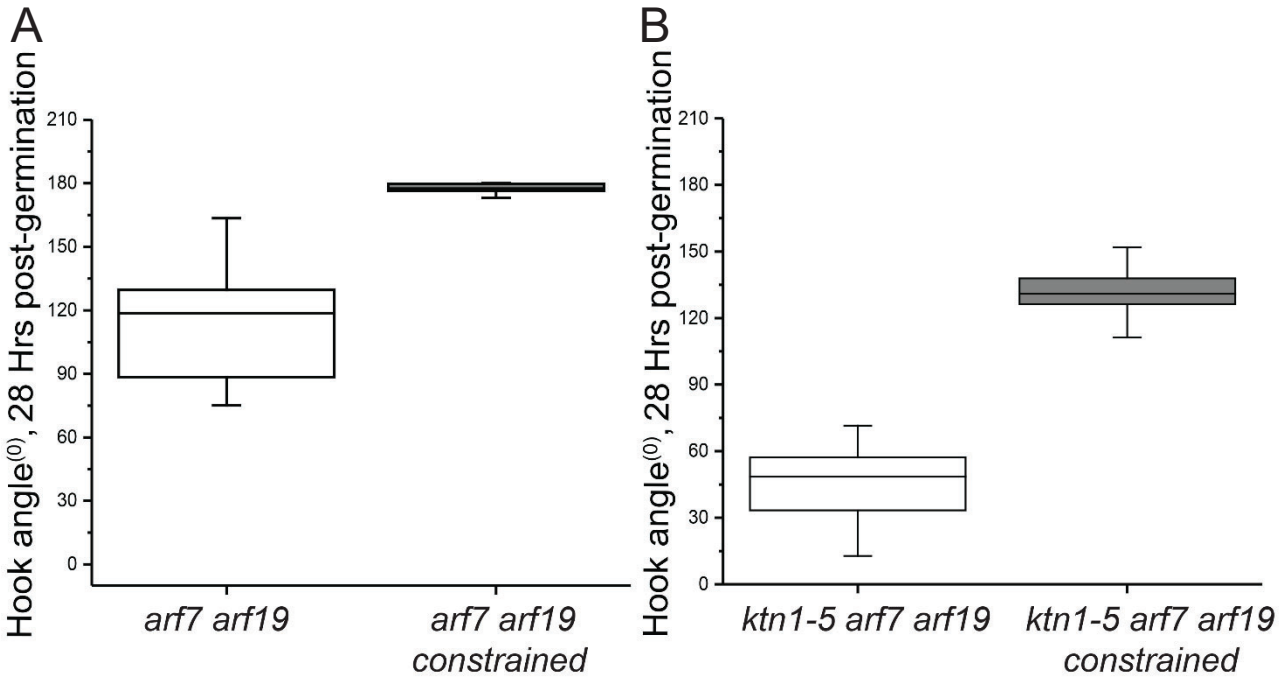

Figure. S7 Mechanically constrained hook formation is not dependent on ARF7 and ARF19. Quantification of apical-hook angles in *arf7 arf19* (A) and *ktn1-5 arf7 arf19* (B) seedlings. growing on the surface of MS agar or growing through the gel (constrained), 28 Hrs after germination, n = 16 seedlings/ group. Box plots showing the first and third quartiles, split by the median; whiskers extend to minimum and maximum values.